

Second-order coherence properties of amplified spontaneous emission

ILIYA V. DORONIN,^{1,2} EVGENY S. ANDRIANOV,^{1,2} ALEXANDER A. ZYABLOVSKY,^{1,2} ALEXANDER A. PUKHOV,^{1,2,3} YURI E. LOZOVIK,^{1,2,4} ALEXEY P. VINOGRADOV,^{1,2,3} AND ALEXANDER A. LISYANSKY^{5,6,*}

¹*Dukhov Research Institute of Automatics, 127055 Moscow, Russia*

²*Moscow Institute of Physics and Technology, 141700 Moscow Region, Russia*

³*Institute for Theoretical and Applied Electromagnetics, 125412 Moscow, Russia*

⁴*Institute of Spectroscopy RAS, 142190 Troitsk, Moscow, Russia*

⁵*Department of Physics, Queens College of the City University of New York, Queens, NY 11367, USA*

⁶*The Graduate Center of the City University of New York, NY 10016, USA*

**Alexander.Lisyansky@qc.cuny.edu*

Abstract: Properties of light sources based on amplified spontaneous emission (ASE) are similar to the properties of lasers in many regards. However, even though ASE has been widely studied, its photon statistics have not been settled. There are no reliable theoretical estimates or unambiguous experimental data for the second-order coherence function of photons that characterizes the coherence properties of a light source. Our computer simulation clearly establishes that, independently of pump power, the light produced by ASE is similar to that of a thermal source. This result lays bare the fundamental difference between ASE radiation and laser radiation.

© 2019 Optical Society of America under the terms of the [OSA Open Access Publishing Agreement](#)

1. Introduction

New luminescent materials with high gain and quantum yield such as perovskites [1–3] have spurred interest in ASE light sources. The narrow linewidth, high intensity of radiation, and low production cost make these light sources attractive for optoelectronic and optical storage devices [4].

ASE or super-luminescence can be produced by an active medium pumped by incoherent radiation. When a luminescent material is pumped, one of the excited atoms spontaneously emits a photon. Before leaving the active medium, this photon triggers stimulated emission of inverted atoms in its path [5–7]. Moreover, a plane wave traveling over an ASE system is amplified: $E(L) \sim \exp[LG(\gamma_p - \gamma_D)/(\gamma_p + \gamma_D)]$, where L is the length of the active medium, G is the gain coefficient which is characteristic of the medium, and γ_p and γ_D are the pump and dissipation rates, respectively [5,8]. Above the compensation threshold, which is determined by the relation $\gamma_p = \gamma_D$, a large increase of the output radiation with an increase in pumping is observed. The saturation of the population inversion $D_0 = (\gamma_p - \gamma_D)/(\gamma_p + \gamma_D)$ results in an S-shaped dependence of the output intensity on the pump rate. The S-shaped of the input-output curve is also characteristic of lasers, in which it arises due to lasing above the laser threshold $\gamma_p(r) = \gamma_{las}$, where r is the reflection coefficient from the resonator walls. For the simplest case of the Fabry-Perot resonator, the generation of coherent light begins if $r^2 \exp[LG(\gamma_p - \gamma_D)/(\gamma_p + \gamma_D)] \geq 1$. This inequality determines the threshold of the pump rate [5,8]. In an ASE system, it is assumed that there is no resonator and even if some reflection at boundaries of an active medium exists, then ASE occurs if $r^2 \exp[LG(\gamma_p - \gamma_D)/(\gamma_p + \gamma_D)] \ll 1$.

Thus, similar to a laser, ASE exhibits threshold behavior. Moreover, ASE sources share many features with conventional lasers. Since, above the threshold, the gain of the active medium has a maximum at the transition frequency of inverted atoms ω_{TLS} , the amplification of the electromagnetic (EM) field at neighboring frequencies is lower. The spectral linewidths of ASE sources are then narrowed when the volume or the gain coefficient of the active medium increases.

One of the most important characteristics of a light source is its photon statistics. The statistical properties of radiation are characterized by the second-order coherence function $g^{(2)}(\tau) = \langle \hat{I}(t)\hat{I}(t+\tau) \rangle / \langle \hat{I}(t) \rangle^2$, where $\hat{I}(t)$ is the operator of radiation intensity and the time t is such that the system has reached a stationary state and its dynamics does not depend on the initial conditions. Coherent laser light has a Poissonian photon distribution with $g^{(2)}(0) = 1$, while black-body radiation and single-photon sources have super- and sub-Poissonian photon distributions for which $g^{(2)}(0)$ equals 2 and 0, respectively [9]. Statistical properties of ASE, however, are not well-studied because the determination of the distribution of emitted photons is complex for a wide spectral range of radiation [10]. The question of the statistics expected for ASE is still not settled. There are arguments that ASE is highly coherent with Poissonian photon statistics ($g^{(2)}(0) = 1$) [11,12], as well as arguments that ASE has low coherency with $g^{(2)}(0) = 2$ [13]. Recent experiments have yielded contradicting results. In [14], it is shown that ASE systems can demonstrate laser-like statistical properties and have $g^{(2)}(0)$ that is close to unity; in [15–17], it is demonstrated that depending on the pump power $g^{(2)}(0)$ changes from 2 to 1, whereas [13,18] reported that $g^{(2)}(0) = 2$ as is characteristic of black-body radiation.

In this paper, we investigate the dependence of the coherence properties of ASE on the pump rate. We demonstrate by computer simulations that ASE has the super-Poissonian distribution of photons with $g^{(2)}(0) \approx 2$ for any value of the pump rate. This makes it possible to distinguish ASE sources from lasers.

2. The model for light interaction with active medium

To describe the interaction between an EM field and atoms of a gain medium we use the Jaynes-Cummings Hamiltonian in the rotating wave approximation [19]:

$$\hat{H} = \sum_n \hbar \omega_n \hat{a}_n^\dagger \hat{a}_n + \sum_j \hbar \omega_{TLS} \hat{\sigma}_j^\dagger \hat{\sigma}_j + \sum_{n,j} \hbar \Omega_{nj} (\hat{a}_n^\dagger \hat{\sigma}_j + \hat{a}_n \hat{\sigma}_j^\dagger) + \hat{H}_R + \hat{H}_{SR}, \quad (1)$$

where \hat{a}_n^\dagger and \hat{a}_n are creation and annihilation operators for the n -th mode of the EM field. These operators satisfy the commutation relation $[\hat{a}_n, \hat{a}_m^\dagger] = \delta_{n,m}$. The electric field operator at the point x_j is expressed as $\hat{\mathbf{E}}(x_j) = \sum_n (\mathbf{E}_n(x_j) \hat{a}_n + h.c.)$, where $\mathbf{E}_n(x) = \sqrt{4\pi\hbar\omega_n/V} \cos(k_n x)$ is the electric field “per one photon” of the n -th mode and V is the volume of the system. Atoms of the active medium are described as two-level systems (TLSs) with the ground, $|g\rangle$, and excited, $|e\rangle$, states; $\hat{\sigma}_j^\dagger = |e_j\rangle\langle g_j|$, $\hat{\sigma}_j = |g_j\rangle\langle e_j|$, and $\hat{D}_j = |e_j\rangle\langle e_j| - |g_j\rangle\langle g_j|$ are raising, lowering, and population inversion operators of the j -th TLS, respectively, and ω_{TLS} is its transition frequency. The third term in Eq. (1) describes the interaction between field modes and dipole moments of TLSs. The coupling constant Ω_{nj}

(the Rabi frequency) is equal to $-\mathbf{E}_n(x_j) \cdot \mathbf{d}_j / \hbar$, where x_j is the position of the j -th TLS and $\mathbf{d}_j = \langle e | \mathbf{e} \mathbf{r} | g \rangle_j$ is the matrix element of its dipole moment.

The first and the second terms of Hamiltonian (1) describe the EM field and the active medium, respectively, the third term is responsible for the interaction between the EM field and atoms, the other two terms describe all essential reservoirs and their interactions with the EM field and the active medium. These reservoirs are critical to our considerations since they describe losses in the system, incoherent pumping of the active medium, and the spontaneous emission. \hat{H}_R is a sum of Hamiltonians of reservoirs:

$$\hat{H}_R = \sum_n \hat{H}_{Ra}^{(n)} + \sum_j \hat{H}_{R\sigma}^{(j)} + \sum_j \hat{H}_{RPump}^{(j)}, \quad (2)$$

where

$$\hat{H}_{Ra}^{(n)} = \sum_m \hbar \omega_{nm}^b \hat{b}_{nm}^\dagger \hat{b}_{nm} \quad (3)$$

describes the reservoir of phonons in waveguide walls coupled with the n -th mode,

$$\hat{H}_{R\sigma}^{(j)} = \sum_m \hbar \omega_{jm}^c \hat{c}_{jm}^\dagger \hat{c}_{jm} \quad (4)$$

is the Hamiltonian of the reservoir of phonons in the active medium coupled with the j -th atom, the operators \hat{b}_{nm} , \hat{c}_{jm} and \hat{b}_{nm}^\dagger , \hat{c}_{jm}^\dagger are annihilation and creation operators of phonons. We assume that every atom of the active medium couples with its own phonon reservoir [8]. This approximation is valid when the coherence length of the phonons is shorter than the distance between atoms of the active medium.

To describe pumping of the active medium atoms, we introduce reservoirs of auxiliary TLSs having negative temperature (see for details [8]). The j -th reservoir interacts with the j -th atom and is described by the Hamiltonian

$$\hat{H}_{RPump}^{(j)} = \sum_m \hbar \omega_{jm}^s \hat{s}_{jm}^\dagger \hat{s}_{jm}, \quad (5)$$

where \hat{s}_{jm} and \hat{s}_{jm}^\dagger are lowering and raising population inversion operators for TLSs in the reservoir with a negative temperature.

The Hamiltonian that describes the interaction of the system with these reservoirs is the sum

$$H_{SR} = \sum_n \hat{H}_{SRa}^{(n)} + \sum_j \hat{H}_{SRdeph}^{(j)} + \sum_j \hat{H}_{SRD}^{(j)} + \sum_j \hat{H}_{SRPump}^{(j)}, \quad (6)$$

where

$$\hat{H}_{SRa}^{(n)} = \sum_m v_{mn} \left(\hat{a}_n \hat{b}_{nm}^\dagger + \hat{a}_n^\dagger \hat{b}_{nm} \right) \quad (7)$$

describes the interaction of phonons in the waveguide walls with photons; the Hamiltonians

$$\hat{H}_{SRdeph}^{(j)} = \sum_m \kappa_{jm} \left(\hat{c}_{jm} + \hat{c}_{jm}^\dagger \right) \hat{\sigma}_j^\dagger \hat{\sigma}_j \quad (8)$$

and

$$\hat{H}_{SRD}^{(j)} = \sum_m \beta_{jm} \left(\hat{c}_{jm} \hat{\sigma}_j^\dagger + \hat{c}_{jm}^\dagger \hat{\sigma}_j \right) \quad (9)$$

describes elastic and inelastic interactions between j -th atom and phonons in the active medium, and

$$\hat{H}_{SRPump}^{(j)} = \sum_m \eta_{jm} (\hat{\sigma}_j \hat{s}_{jm}^\dagger + \hat{\sigma}_j^\dagger \hat{s}_{jm}) \quad (10)$$

is the Hamiltonian of the interaction between the j -th atom of the active medium and the reservoir with a negative temperature, which describes incoherent pumping. Below we use Heisenberg representation of the operators.

To obtain the Heisenberg-Langevin equation of motion for the relevant operators of the system, we eliminate the reservoir variables by averaging over the equilibrium states of the reservoirs [19]. In the process of averaging, we assume that, first, the reservoir is much larger than the system, and therefore, one can neglect the influence of the system on the reservoir. Second, since the timescale, characterizing fluctuations in the reservoir ($\tau_R \sim \hbar / kT \sim 10^{-14}$ s [19]), is much shorter than the relaxation time of the system (for a typical gain medium, such as organic semiconductors, the relaxation time is about 10^{-13} s), the fluctuation-dissipation theorem is correct. Consequently, after averaging, both relaxation and noise terms appear in the equations.

The elimination of the reservoir variables, \hat{b}_{nm} , \hat{s}_{jm} , and \hat{c}_{jm} , results in the appearance of the relaxation, γ_a , γ_D , γ_{deph} , γ_p , and fluctuation (noise) terms, \hat{F}_{an} , \hat{F}_{an}^\dagger , \hat{F}_{σ_j} , $\hat{F}_{\sigma_j}^\dagger$, and \hat{F}_{D_j} , in the equation for the operators \hat{a}_n^\dagger , \hat{a}_n , $\hat{\sigma}_j^\dagger$, $\hat{\sigma}_j$, and \hat{D}_j (see [8,19]). Note that the corresponding terms are connected via the fluctuation-dissipation theorem. The elimination of \hat{b}_{nm} results in the appearance of γ_a and \hat{F}_{an} ; the elimination of \hat{c}_{jm} leads to the appearance of γ_{deph} and \hat{F}'_{σ_j} ; the elimination of \hat{h}_{jm} leads to the appearance of γ_{deph} , \hat{F}'_{σ_j} , γ_D , \hat{F}''_{σ_j} and \hat{F}''_{D_j} . By introducing new noise terms $\hat{F}_{\sigma_j} = \hat{F}'_{\sigma_j} + \hat{F}''_{\sigma_j} + \hat{F}'''_{\sigma_j}$ and $\hat{F}_{D_j} = \hat{F}''_{D_j} + \hat{F}'''_{D_j}$, we can rewrite the final equations for the operators \hat{a}_n^\dagger , \hat{a}_n , $\hat{\sigma}_j^\dagger$, $\hat{\sigma}_j$, and \hat{D}_j as follows:

$$\frac{d}{dt} \hat{a}_n = (-\gamma_a / 2 - i\Delta_n) \hat{a}_n - i \sum_j \Omega_{nj} \hat{\sigma}_j + \hat{F}_{an}, \quad (11)$$

$$\frac{d}{dt} \hat{a}_n^\dagger = (-\gamma_a / 2 + i\Delta_n) \hat{a}_n^\dagger + i \sum_j \Omega_{nj} \hat{\sigma}_j^\dagger + \hat{F}_{an}^\dagger, \quad (12)$$

$$\frac{d}{dt} \hat{\sigma}_j = -\hat{\sigma}_j (\gamma_p + \gamma_D + \gamma_{deph}) / 2 + i \sum_n \Omega_{nj} \hat{a}_n \hat{D}_j + \hat{F}_{\sigma_j}, \quad (13)$$

$$\frac{d}{dt} \hat{\sigma}_j^\dagger = -\hat{\sigma}_j^\dagger (\gamma_p + \gamma_D + \gamma_{deph}) / 2 - i \sum_n \Omega_{nj} \hat{a}_n^\dagger \hat{D}_j + \hat{F}_{\sigma_j}^\dagger, \quad (14)$$

$$\frac{d}{dt} \hat{D}_j = -\gamma_p (\hat{D}_j - 1) - \gamma_D (\hat{D}_j + 1) + 2i \sum_n \Omega_{nj} (\hat{a}_n^\dagger \hat{\sigma}_j - \hat{a}_n \hat{\sigma}_j^\dagger) + \hat{F}_{D_j}, \quad (15)$$

where $\Delta_n = \omega_n - \omega_{TLS}$.

In Eq. (15), the term $-\gamma_p (\hat{D}_j - 1)$ describes pumping that increases the expectation value of the population inversion operator \hat{D}_j to 1, while the term $-\gamma_D (\hat{D}_j + 1)$ describes relaxation that decreases $\langle \hat{D}_j \rangle$ to -1 . After simple algebra, Eq. (15) may be recast as

$$\frac{d}{dt} \hat{D}_j = -(\gamma_p + \gamma_D)(\hat{D}_j - D_0) + 2i \sum_n \Omega_{nj} (\hat{a}_n^\dagger \hat{\sigma}_j - \hat{a}_n \hat{\sigma}_j^\dagger) + \hat{F}_{Dj},$$

where $D_0 = (\gamma_p - \gamma_D) / (\gamma_p + \gamma_D)$. In the stationary solution, the inverse population $\langle \hat{D}_j \rangle$ approaches $D_0 = (\gamma_p - \gamma_D) / (\gamma_p + \gamma_D)$ from below.

Since each atom of the active medium interacts with its own environment described by the corresponding phonon reservoir, the correlation functions of noise operators of different atoms are assumed to be equal to zero [8], i.e.

$$\langle \hat{F}_i(t) \hat{F}_j(t') \rangle \sim \delta_{ij}. \tag{16}$$

The correlation functions of the noise operators of Eqs. (11)-(15) are

$$\langle \hat{F}_{an}^\dagger(t') \hat{F}_{an}(t) \rangle = 2\gamma_a \bar{n}(\omega_n) \delta_{nm} \delta(t-t'), \tag{17}$$

$$\langle \hat{F}_{\sigma_j}(t) \hat{F}_{\sigma_j}(t') \rangle = i \left\langle \hat{\sigma}_j \sum_k \hat{a}_k \Omega_{kj} \right\rangle \delta(t-t'), \tag{18}$$

$$\langle \hat{F}_{\sigma_j}^\dagger(t) \hat{F}_{\sigma_j}^\dagger(t') \rangle = -i \left\langle \sum_k \hat{\sigma}_j^\dagger \hat{a}_k^\dagger \Omega_{kj} \right\rangle \delta(t-t'), \tag{19}$$

$$\langle \hat{F}_{\sigma_j}^\dagger(t) \hat{F}_{\sigma_j}(t') \rangle = \frac{1}{2} \left[\gamma_p + \gamma_{ph} (1 + \langle \hat{D}_j \rangle) \right] \delta(t-t'), \tag{20}$$

$$\langle \hat{F}_{Dj}(t) \hat{F}_{Dj}(t') \rangle = \left[(\gamma_D + \gamma_p)(D_0 - \langle \hat{D}_j \rangle) + 2 \sum_k \Omega_{kj} (\langle \hat{a}_k^\dagger \hat{\sigma}_j - \hat{a}_k \hat{\sigma}_j^\dagger \rangle) \right] \delta(t-t'), \tag{21}$$

where $\bar{n}(\omega) = (\exp(\hbar\omega/kT) - 1)^{-1}$ is the mean number of excitations in reservoir (7).

Because in the optical region $\bar{n}(\omega) \ll 1$, below we do not take into account \hat{F}_{an} and \hat{F}_{an}^\dagger .

Since in most ASE experiments, the number N_c of inverted atoms even in a subwavelength volume is large (e.g., in a volume about 100 nm in extent, N_c is of the order of 10^3), we can transition from operators to c -numbers. For this purpose, we use the method of large cells. We divide the whole volume into cells of the size $\lambda_{TLS} / 10$ (λ_{TLS} is the transition wavelength of gain medium atoms) and switch to the mean operators: $\hat{\sigma}_k^{cell\dagger} = \sum_{j \in cell_k} \hat{\sigma}_j^\dagger / N_c$, $\hat{\sigma}_k^{cell} = \sum_{j \in cell_k} \hat{\sigma}_j / N_c$, and $\hat{D}_k^{cell} = \sum_{j \in cell_k} \hat{D}_j / N_c$. Following the method of the system size expansion [19], we consider $1/N_c$ as an expansion parameter and investigate the limiting behavior of the system when $N_c \rightarrow \infty$, neglecting higher-order terms with respect to $1/N_c$ terms. In this limit, the expected values of operators grow with N_c faster than the quantum corrections to these expected values. This enables us to transform Eqs. (11)–(15) to a system of equations for c -numbers in the leading order of $1/N_c$, while quantum corrections can be presented as a classical noise in the second order of $1/N_c$.

Since the cell size is smaller than the wavelength of radiation, we assume that the Rabi frequency is the same for all the atoms in the cell. For the n -th mode and the k -th cell, $\Omega_{nj} = \Omega_{nk}$ for any j -th atom of the cell. The corresponding terms in Eqs. (11) and (12) become $\sum_{j \in cell_k} \Omega_{nj} \hat{\sigma}_j = \Omega_{nk} N_c \hat{\sigma}_k^{cell}$, where $\Omega_{nk} = -\mathbf{d}_{egk} \cdot \mathbf{E}_n(x_k) / \hbar$, x_k is the coordinate of

the k -th cell and \mathbf{d}_{egk} is the transition dipole moment of atoms averaged over the k -th cell. Finally, we obtain the system of equations for c -numbers:

$$\frac{da_n}{dt} = (-\gamma_a / 2 - i\Delta_n) a_n - i \sum_k \Omega_{nk} N_c \sigma_k^{cell}, \quad (22)$$

$$\frac{da_n^{cc}}{dt} = (-\gamma_a / 2 + i\Delta_n) a_n^{cc} + i \sum_k \Omega_{nk} N_c \sigma_k^{cell cc}, \quad (23)$$

$$\frac{d\sigma_k^{cell}}{dt} = -\sigma_k^{cell} (\gamma_p + \gamma_D + \gamma_{deph}) / 2 + i \sum_n \Omega_{nk} a_n D_k^{cell} + F_k^{\sigma^{cell}}, \quad (24)$$

$$\frac{d\sigma_k^{cell cc}}{dt} = -\sigma_k^{cell cc} (\gamma_p + \gamma_D + \gamma_{deph}) / 2 - i \sum_n \Omega_{nk} a_n^{cc} D_k^{cell} + F_k^{\sigma^{cell cc}}, \quad (25)$$

$$\frac{dD_k^{cell}}{dt} = -(\gamma_p + \gamma_D) (D_k^{cell} - D_0) + 2i \sum_n \Omega_{nk} (a_n^{cc} \sigma_k^{cell} - a_n \sigma_k^{cell cc}) + F_k^{D^{cell}}. \quad (26)$$

In these equations, the unknown variables are denoted by the same letters as the corresponding operators except for operators \hat{a}_n^\dagger and $\hat{\sigma}_k^{cell \dagger}$. The latter operators are replaced by the c -numbers a_n^{cc} and $\sigma_k^{cell cc}$. The last terms in Eqs. (24)-(26) describe classical noises; their correlation functions are similar to the correlation functions for the operators, see Eqs. (17)-(21) [8].

In the absence of noise terms in Eqs. (24)-(26), Eqs. (22) and (23) and Eqs. (24) and (25) are complex conjugates. If initially $a_n^{cc}(t=0) = (a_n(t=0))^*$ and $\sigma_k^{cell cc}(t=0) = (\sigma_k^{cell}(t=0))^*$, then these variables remain complex-conjugated all the time. Since operators \hat{a}_n^\dagger , \hat{a}_n and $\hat{\sigma}_k^{cell \dagger}$, $\hat{\sigma}_k^{cell}$ do not commute, in Eqs. (24)-(25), one needs to consider different realizations for noises. Consequently, c -number noise terms corresponding to conjugated operators though retain correct correlations properties are no longer complex conjugated [8,19]. Then, Eqs. (22) and (23) and Eqs. (24) and (25) are also not complex conjugates. As a result, the variables a_n^{cc} , a_n and $\sigma_k^{cell cc}$, σ_k^{cell} corresponding to the operators \hat{a}_n^\dagger , \hat{a}_n and $\hat{\sigma}_k^{cell \dagger}$, $\hat{\sigma}_k^{cell}$ cease to be complex conjugates.

3. Computer simulation of ASE

As a model for ASE source, we use a 1D waveguide of length $L_0 = 1800\lambda_{TLS}$ which contains a region of length $L = 140\lambda_{TLS}$ filled with gain medium atoms, $\lambda_{TLS} = 2\pi c / \omega_{TLS}$. Pumping of this region creates a positive population inversion (see Fig. 1).



Fig. 1. The sketch of the ASE source based on a single-mode waveguide. The active medium in the central region of the waveguide (shaded by red) with the length L is pumped by an external source; the active medium outside of this region is not pumped.

In our numerical simulation, the EM field is modeled by 600 modes with equidistant frequencies within the interval $(0.92\omega_{TLS}, 1.08\omega_{TLS})$. The gain medium is divided into

subwavelength simulation cells of size $\Delta x = \lambda/10$ (the total number of cells is 1400). To verify the validity of the chosen parameters for the computational scheme, namely, the lengths of the waveguide and the active medium cells, we compared the results of simulations for various values of L_0 and Δx . We confirmed that an increase in the waveguide length above $1800\lambda_{TLS}$, as well as a decrease of the cell size below $\lambda/10$, did not affect the results of the simulation. We use Eqs. (22)-(26) to find the radiation output, the spectrum, and the second-order coherence function of ASE and laser radiations. Variations in dissipation rates can be compensated for by changes in the pump rate. Therefore, in calculations, the parameters in Eqs. (22)-(26) are chosen to be close to the gain medium based on organic semiconductors [20], while the pump rates are varied over the wide range. The relaxation rates are $\gamma_a = 2 \times 10^{-3} \omega_{TLS}$, $\gamma_{deph} = 5.2 \times 10^{-2} \omega_{TLS}$, $\gamma_D = 10^{-6} \omega_{TLS}$, and the pump rate varies within the interval $\gamma_p = (2 \times 10^{-7} - 10^{-2}) \omega_{TLS}$. Such a choice of the modeled medium means that lasing may start if $r^2 = \exp[-LG(\gamma_p - \gamma_D)/(\gamma_p + \gamma_D)] \sim 0.05$, and ASE is observable if $|r|^2 < 0.05$.

As mentioned above, the main characteristic that allows one to distinguish coherent laser radiation from incoherent black-body radiation experimentally is the second-order coherence function $g^{(2)}(\tau)$. The value of $g^{(2)}(\tau)$ for any radiation source tends to unity as $\tau \geq 1/\Delta\omega$, where $\Delta\omega$ is the radiation linewidth of the source [9,19]. Consequently, the response time τ_{res} of an experimental setup should be smaller than $1/\Delta\omega$. If $\tau_{res} > 1/\Delta\omega$, the measured value of $g^{(2)}(0)$ is always about unity. Experimentally, a spectrum of an investigated source is narrowed by filtering. It is preferable to narrow the line as much as possible. For this reason, we study the second-order coherence function at a fixed frequency, $g^{(2)}(\omega, \tau) = \langle I_\omega(t)I_\omega(t+\tau) \rangle / \langle I_\omega(t) \rangle^2$, where I_ω is the output intensity at the frequency ω . Representing the electric field operator as $\hat{\mathbf{E}}(x, t) = \hat{\mathbf{E}}^{(+)}(x, t) + \hat{\mathbf{E}}^{(-)}(x, t)$, where $\hat{\mathbf{E}}^{(+)}(x, t) = \sum_n \mathbf{E}_n(x) \hat{a}_n(t)$, and $\hat{\mathbf{E}}^{(-)}(x, t) = \sum_n \mathbf{E}_n^*(x) \hat{a}_n^\dagger(t)$, for the average intensity of the electromagnetic field, $\langle I(x, t) \rangle = \langle \hat{\mathbf{E}}^{(-)}(x, t) \hat{\mathbf{E}}^{(+)}(x, t) \rangle$ [9], we arrive at the following expression for $g^{(2)}(\omega_n, \tau)$:

$$g^{(2)}(\omega_n, \tau) = \frac{\langle \hat{a}_n^\dagger(t) \hat{a}_n^\dagger(t+\tau) \hat{a}_n(t+\tau) \hat{a}_n(t) \rangle}{\langle \hat{a}_n^\dagger(t+\tau) \hat{a}_n(t+\tau) \rangle \langle \hat{a}_n^\dagger(t) \hat{a}_n(t) \rangle}. \quad (27)$$

After the transition to c -numbers, we calculate $g^{(2)}(\omega_n, \tau)$ at $\tau = 0$ as $\langle a_n^{cc}(t) a_n^{cc}(t) a_n(t) a_n(t) \rangle / \langle a_n^{cc}(t) a_n(t) \rangle^2$, where averaging is performed over different realizations after the corresponding mean values reach the stationary values. For this purpose, we find the stationary state of the system without noises utilizing the Runge-Kutta scheme [21]. Then we consider these stationary values as initial conditions and solve Eqs. (22)-(26) with the noise terms. At this calculation stage, we use the Euler scheme, which is stable near the stationary state [21,22].

Our numerical simulation confirms that the input-output curve of the ASE source has an S -shape (the blue line in Fig. 2) similar to the intensity of conventional laser radiation. The S -shape of the input-output curve of ASE sources arises due to the three regimes of the system behavior corresponding to different pump rates. At a low pump power, the energy loss of the EM wave propagating in the waveguide exceeds its gain in the active medium. In this regime,

the EM wave exponentially decays while propagating through the structure; the output power linearly increases with the growth of the pump power. At a higher pump power, the gain exceeds the propagation losses, and the propagating EM wave exponentially intensifies. At this regime, the saturation of the active medium is inessential. This regime corresponds to the shaded area in Fig. 2. A further increase in the pump rate leads to saturation of the active medium (see Fig. 2). The transitional region between the first and third regimes is referred to as the ASE threshold [5]. Note that in all three regimes, $g^{(2)}(\omega_{TLS}, 0)$ remains equal to 2 (see Fig. 2.)

In the third region, the decrease of intensity happens because incoherent pumping not only increases D but also causes additional dephasing of the atom dipole moments [see Eq. (24)]. As a result, the stationary value of the dipole moment of atoms of the active medium, σ^{cell} , is inversely proportional to the sum $\gamma_{deph} + \gamma_p + \gamma_D$. In this sum, the relaxation rate of the atomic dipole moment, γ_{deph} , and the relaxation rate of population inversion, γ_D , describe the dephasing that arises due to the interaction of active atoms with phonons, while the pump rate of active atoms, γ_p , describes the dephasing arising due to incoherent pumping. For pumping rates γ_p , which are much greater than both γ_{deph} and γ_D , the stationary value of the dipole moments of atoms of the active medium is inversely proportional to the pumping rate, $\sigma^{cell} \sim 1/\gamma_p$. The output power is proportional to $|\sigma^{cell}|^2$ and therefore, when the pump rate tends to infinity, the output power monotonically decreases [23], as seen Fig. 2. In this region, $g^{(2)}(\omega, 0)$ also remains equal to 2 for any frequency.

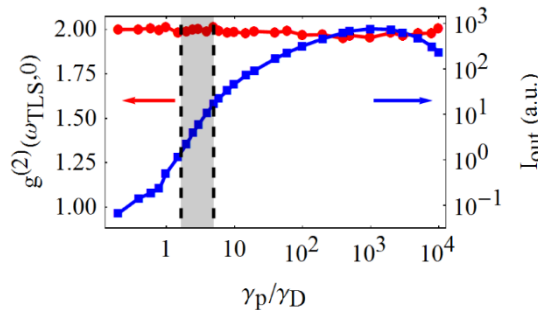


Fig. 2. The intensity of the EM field at the boundary of the active medium (the blue line) and $g^{(2)}(\omega_{TLS}, 0)$ (the red line). The left vertical dashed line shows the compensation threshold, at which pumping compensates for losses in the active medium. The right vertical dashed line represents the pump rate, at which the system transitions to the nonlinear regime due to substantial saturation of the active medium. In this regime, the output power linearly depends on the pump power [5]. The shaded area shows the transitional region in which an increase in the pump rate results in an exponential increase in the radiation intensity.

Though, within the transition range, the output intensity increases by more than an order of magnitude (see the blue line in Fig. 2), the value of the second-order coherence function of ASE is independent of the pump rate and the frequency (see the red line in Fig. 2) and is about 2, while for coherent light it should be equal to 1.

In Figs. 3(a),(c) and 3(b),(d), the spectral distribution of the photon number, $n(\omega) = \langle a^{cc}(\omega)a(\omega) \rangle / \langle a^{cc}(\omega)a(\omega) \rangle_{\max}$, and $g^{(2)}(\omega, 0)$ are shown at the pump rates below and above the compensation threshold, respectively. For small pump rates, the spectrum of the system is similar to the spectrum of a single atom of the active medium, see Fig. 3(a). For pump rates that are higher than that of the transitional regime, the spectrum of the system

markedly narrows, Fig. 3(c). The observed narrowing is a common feature for both lasers and ASE.

At the same time, we can see that despite the narrowing of the spectrum line, $g^{(2)}(\omega, 0) \approx 2.0$ for any mode, independently of the frequency [see Figs. 3(b) and 3(d)]. As we discuss below, this distinguishes ASE from laser radiation. Visible fluctuations of $g^{(2)}(\omega, 0)$ are due to the finite number of realizations of stochastic process used in the calculations.

As Figs. 2 and 3(b),(d) show, the second-order coherence function $g^{(2)}(\omega, 0)$ depends on neither the pump rate nor the frequency, and it is about 2. This means that the coherent properties of ASE are substantially different from radiation of lasers; they are rather close to the black-body radiation.

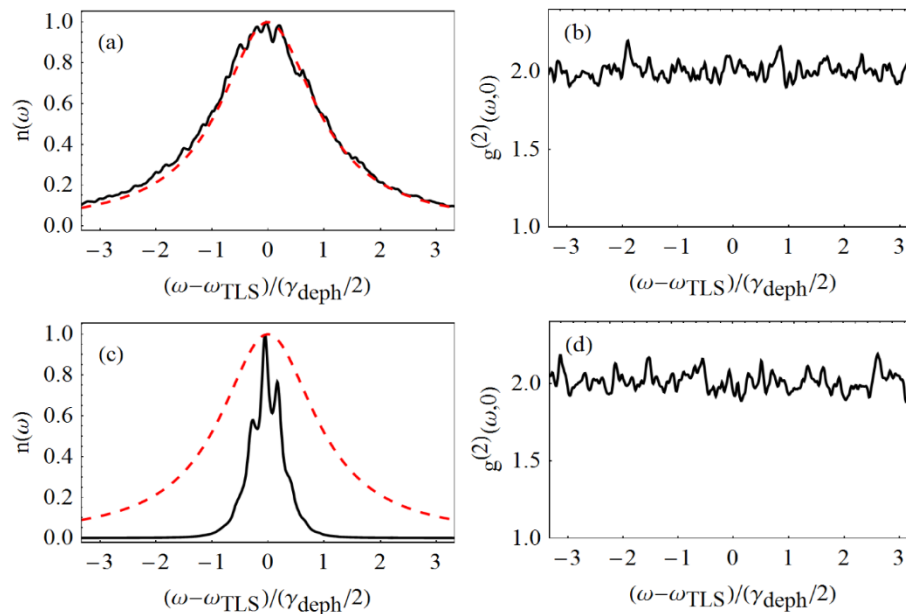


Fig. 3. Spectra, $n(\omega)$, normalized by its maximum value, and $g^{(2)}(\omega, 0)$ of an ASE source for the pump rates below (a), (b) and above (c), (d) the compensation threshold. In Figs. (a) and (b), the pump rate γ_p is equal to γ_D , and in Figs. (c) and (d), it is equal to $20\gamma_D$. Dashed red curves show the absorption line of the unpumped medium. The values of $g^{(2)}(\omega, 0)$ are found by using Eq. (27).

4. Laser emission

To test our results, in the system shown in Fig. 1, we add mirrors to the edges of the active medium and make calculations similar to that discussed above. The mirrors introduce positive feedback, and the system is expected to lase. In a laser, the value of $g^{(2)}(0)$ depends on the pump rate [9]: below the generation threshold, $g^{(2)}(0)$ must be close to two, above the threshold, it should tend to one. Our computer simulation confirms this assumption.

In Fig. 4, the dependence of the system output intensity on the pump rate is shown. This dependence has a pronounced S-shape (the blue line). The laser generation threshold (an inflection on the S-shaped curve) arises due to three regimes of a laser. For small pump rates, the amplification of radiation in the gain medium is not sufficient for the loss compensation in the waveguide and mirrors. In this regime, auto-oscillations are not established. For

intermediate pump rates, auto-oscillations begin, but the nonlinear contribution is not dominant yet. The beginning of auto-oscillations is defined by the Maxwell-Bloch threshold in a system without noise. At a further increase in the pump rate, the population inversion of the active medium becomes significant causing the transition of the dependence of the radiation intensity from exponential to linear.

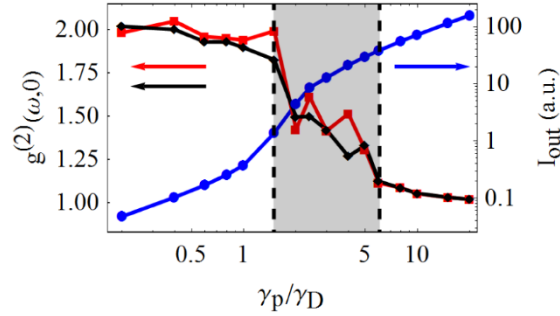


Fig. 4. Red and black curves represent the coherence function $g^{(2)}(\omega, 0)$ for the dominant modes shown in Fig. 5(c). The blue curve is the generation curve of the laser. The curves are obtained by solving the Maxwell-Bloch equations with noise. The left vertical dashed line shows the lasing threshold given by the Maxwell-Bloch equations without noise. The right vertical dashed line corresponds to the pump rate, for which $g^{(2)}(\omega, 0) - 1$ of the modes becomes inversely-proportional to the average number of photons. Grey shading marks the transitional regime of the laser. The parameters of the active structure are the same as for the ASE system discussed above. The amplitude reflectance of the mirrors is 0.8.

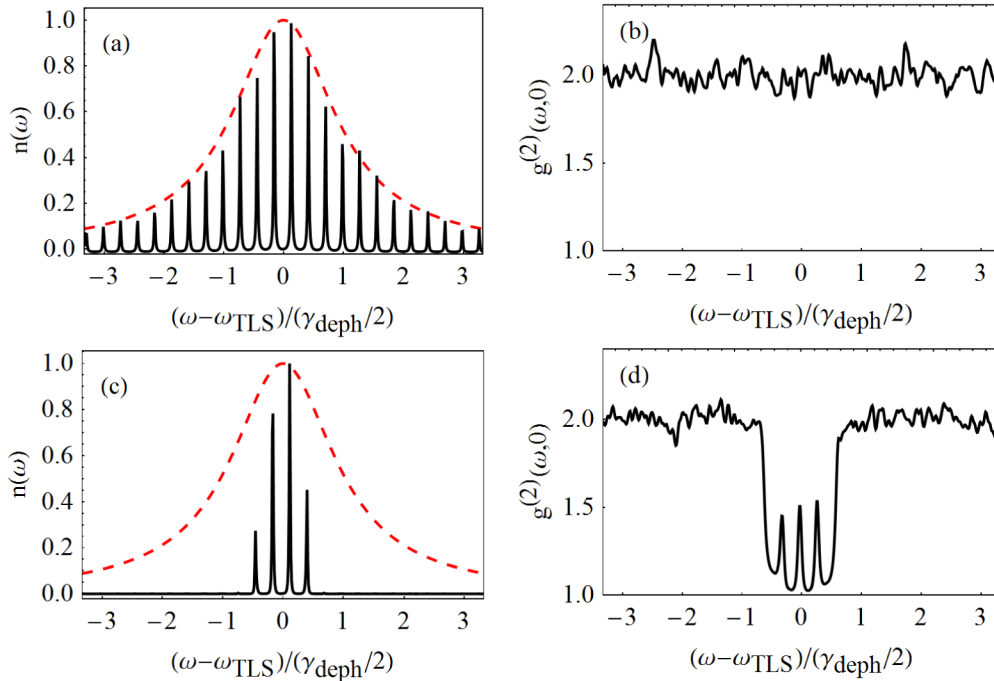


Fig. 5. Normalized spectra and $g^{(2)}(\omega, 0)$ of laser emission for pump rates $\gamma_p = \gamma_D$ (a), (b) (below the lasing threshold) and $\gamma_p = 20\gamma_D$ (c), (d) (above the laser threshold).

Below the generation threshold, the system spectrum exhibits a large number of lines corresponding to modes of the Fabry-Perot cavity [see Fig. 5(a)]. The value of $g^{(2)}(\omega, 0)$ for all modes is approximately 2 [see Fig. 5(b)]. This is close to $g^{(2)}(\omega, 0)$ for the system without mirrors [see Fig. 3(b)]. Far above the generation threshold, there are only a few lines in the spectrum [see Fig. 5(c)]. These lines correspond to the eigenfrequencies of the Fabry-Perot cavity that are closest to the transition frequency of the active medium, and consequently, have the lowest values of thresholds. For these modes, $g^{(2)}(\omega, 0)$ is close to 1 even though for all other modes it remains close to 2.

Near the generation threshold, our model exhibits large fluctuations and a large spread in $g^{(2)}(\omega, 0)$. This happens because, near the threshold, the laser behavior is similar to a second order phase transition [8,19], in which a system undergoes strong fluctuations near the critical point [24]. In our case, the critical region corresponds to pump rates between $\gamma_p = 1.5\gamma_D$ and $6\gamma_D$ (the shaded area in Fig. 4).

Thus, in the system with mirrors, a pronounced generation threshold is observed. Our calculations show that below the threshold, for all modes, $g^{(2)}(\omega, 0)$ significantly exceeds 1, while above the threshold, for the modes in which generation occurs, $g^{(2)}(\omega, 0)$ tends to unity. $g^{(2)}(\omega, 0)$ decreases only for the eigenmodes of the system with mirrors and only when there is coherent feedback. This is in agreement with the expected behavior of a laser. We emphasize that in this section we use exactly the same model as in the previous one except that mirrors that create a cavity are added. Then, using the same procedure as in the previous section, we obtain well-known results. This can serve as a confirmation of the correctness of the results obtained for ASE.

5. Discussion and conclusion

In this paper, we compare the coherent properties of a mirrorless ASE system to the properties of a laser built of the same pumped atoms. To make this comparison, it is convenient to use the parameter $\eta = GD_0L$. At the transition frequency, the gain is $G = 4\pi\omega_{TLS} |\mathbf{d}_j|^2 n_{TLS} / (\hbar\gamma_{deph} c)$, where n_{TLS} is the concentration of the atoms of active medium (see [25,26]).

Since the refractive index of the active medium $\sqrt{\epsilon_{gain}(\omega)}$ differs from the refractive index of vacuum, the reflection from boundaries results in the appearing a Fabry-Perot cavity that, in turn, may cause lasing. The lasing threshold is determined by the following condition [25]:

$$\left| \frac{\sqrt{\epsilon_{gain}(\omega)} - 1}{\sqrt{\epsilon_{gain}(\omega)} + 1} \right| \exp(GDL/2) = 1, \quad (28)$$

The gain is easily expressed through the refractive index $G = -2\omega \text{Im} \sqrt{\epsilon_{gain}(\omega)} / c \approx -\omega \text{Im} \epsilon_{gain}(\omega) / c$. In our computer simulation, the parameter η has not exceeded 5.6. For the considered values of the parameter η , criterion (28) is not satisfied. We, therefore, conclude that our system should produce ASE.

In our 1D model, each atom radiates in both directions forming incident and refracted waves. Therefore, the difference in refractive indices is automatically taken into account. Thus, the independence of $g^{(2)}(\omega, 0) \sim 2.0$ on the pump rate and the frequency (see Fig. 2) indicates that lasing is not achieved, and our system may be considered as mirrorless ASE.

An addition of semi-transparent mirrors with $r = 0.8$ to the boundaries of the active medium with $\eta = 5.6$ converts the system into a laser. As one can see from Fig. 4, for this laser, $g^{(2)}(\omega, 0)$ tends to unity above the laser threshold.

In [15], it has been reported that for a commercial superluminescent light diode (SLD), the value of $g^{(2)}(0)$ tends to unity with an increase in the pump rate. SLDs are high intensity light sources having a broad spectrum in the output radiation. This type of light source is required for a number of applications [27-29]. Since, even for multimode lasers, the spectra are modulated by lines of Fabry-Perot modes, SLDs are manufactured as ASE systems with high gain. To achieve this, special efforts are taken to reduce reflections inside an SLD. A broad spectrum of the SLD output radiation is often considered as the criterion confirming that an SLD operates as an ASE system [30, 31]. According to [30, 31], to eliminate the spectrum modulation by lines of Fabry-Perot modes, the intrinsic reflection coefficient, $|r|^2$, should be less than $2.5 \cdot 10^{-6}$. Thus, if $|r|^2 < 2.5 \cdot 10^{-6}$, the SLD may be considered as an ASE system.

In fact, the definition of ASE as the absence of the spectrum modulations is not quite correct. Indeed, for high gain, lasing may start at an even lower value of the reflection coefficient and before the spectrum becomes modulated. For such a small value of the reflection coefficient, the Q-factor of modes is also low, and the linewidth of the modes may be much greater than the distance between them. This means that the modulation in the spectrum is smoothed. For an SLD, a typical value of the gain is $G \sim 1500 \text{ cm}^{-1}$ [20], with the size of active medium of $L \sim 0.01 \text{ cm}$. In such a system, the lasing may start at $|r|^2 = \exp(-GL) \sim 3 \cdot 10^{-7}$. Thus, the system considered in [15] could be a laser with $g^{(2)}(0) \rightarrow 1$.

To verify this assumption, we perform computer simulation for our model with increased length of the region filled with gain medium atoms. The linear stability analysis of the system shows the existence of the Hopf bifurcation with a lasing solution at the threshold value of the population inversion. The results of computer simulation shown in Fig. 6(a), demonstrate that $g^{(2)}(\omega_{TLS}, 0)$ starts decreasing above the lasing threshold while the spectrum width remains constant. The spectrum remains almost without modulation, and for 600 modes taken into account we observe only a weak ripple near ω_{TLS} [see Fig. 6(b)]. Note that an addition of mirrors with high reflection coefficient causes intense modulation of the spectrum shown in Fig. 5(c).

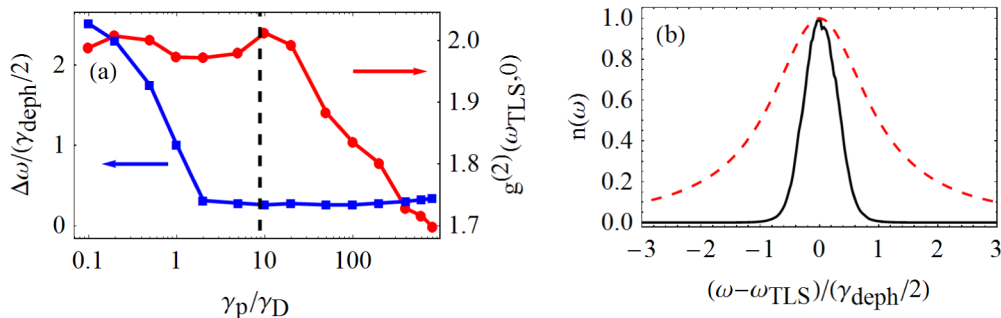


Fig. 6. (a) The dependence of ($g^{(2)}(\omega_{\text{TLS}}, 0)$ the red line) and the spectrum half-width at the half-height $\Delta\omega$ (the blue line) on the pump rate for the mirrorless system with $L = 700\lambda_{\text{TLS}}$ and

$G = 673 \text{ cm}^{-1}$; the dashed black line denotes the lasing threshold derived from linear analysis, $\gamma_p = 8.66 \gamma_D$; the threshold value of the population inversion is $D_n = 0.793$. (b) The normalized spectrum of the system at $\gamma_p = 800 \gamma_D$ (the black solid line) and the spectrum of the atom (the red dashed line).

Thus, according to our calculations, for $\eta \sim 5$, above the compensation threshold, coherence properties of ASE are still characterized by $g^{(2)}(\omega, 0) \approx 2$.

It is interesting to study the value of $g^{(2)}(0)$ for EM waves amplified by stimulated emission in interstellar gases [32–34] and planetary atmospheres [35,36]. Such radiation sources are called astrophysical masers or lasers. In [34, 37], it is claimed that such sources operate as random lasers and should have $g^{(2)}(0) \approx 1$. An alternative mechanism could be the phenomenon of ASE [38] with $g^{(2)}(0) \approx 2$. An investigation of the second-order coherence function of radiation from an astrophysical “maser” could shed light on the mechanism of formation of such sources. In turn, the understanding of the mechanism of the formation of astrophysical masers and lasers can enable one to estimate the concentration of the molecules, atoms, or ions in interstellar clouds.

In addition to its fundamental significance, the difference between ASE and laser radiation is of practical importance. For ghost imaging applications, light sources with super-Poissonian distributions of photons, a narrow linewidth, and a high intensity are required [39]. Currently, either lasers with rotating ground glass [40–42], producing radiation with $g^{(2)}(0)$ between 1.25 and 1.9, or incoherent lamps with a frequency filter [43,44] with $g^{(2)}(0)$ of about 1.05 are used as light sources. In this paper, we demonstrate that the second-order coherence function of ASE sources is about 2 that is closer to the coherence of lasers with rotating ground glass. However, ASE sources are much simpler and easier to manufacture than lasers. This makes ASE light sources promising for ghost imaging.

Funding

National Science Foundation (DMR-1312707); Foundation for the advancement of theoretical physics and mathematics “Basis” (Junior PostDoc grant).

Acknowledgments

We thank V. I. Balykin for helpful discussions.

References

1. G. Xing, N. Mathews, S. S. Lim, N. Yantara, X. Liu, D. Sabba, M. Grätzel, S. Mhaisalkar, and T. C. Sum, “Low-temperature solution-processed wavelength-tunable perovskites for lasing,” *Nat. Mater.* **13**(5), 476–480 (2014).
2. F. Deschler, M. Price, S. Pathak, L. E. Klintberg, D. D. Jarausch, R. Higler, S. Hüttner, T. Leijtens, S. D. Stranks, H. J. Snaith, M. Atatüre, R. T. Phillips, and R. H. Friend, “High photoluminescence efficiency and optically pumped lasing in solution-processed mixed halide perovskite semiconductors,” *J. Phys. Chem. Lett.* **5**(8), 1421–1426 (2014).
3. H. Zhu, Y. Fu, F. Meng, X. Wu, Z. Gong, Q. Ding, M. V. Gustafsson, M. T. Trinh, S. Jin, and X. Y. Zhu, “Lead halide perovskite nanowire lasers with low lasing thresholds and high quality factors,” *Nat. Mater.* **14**(6), 636–642 (2015).
4. A. Nurmikko, “What future for quantum dot-based light emitters?” *Nat. Nanotechnol.* **10**(12), 1001–1004 (2015).
5. A. E. Siegman, *Lasers* (University Science Books, 1986).
6. U. Ganiel, A. Hardy, G. Neumann, and D. Treves, “Amplified spontaneous emission and signal amplification in dye-laser systems,” *IEEE J. Quantum Electron.* **11**(11), 881–892 (1975).
7. S. Yakunin, L. Protesescu, F. Krieg, M. I. Bodnarchuk, G. Nedelcu, M. Humer, G. De Luca, M. Fiebig, W. Heiss, and M. V. Kovalenko, “Low-threshold amplified spontaneous emission and lasing from colloidal nanocrystals of caesium lead halide perovskites,” *Nat. Commun.* **6**(1), 8056 (2015).
8. H. Haken, *Laser light dynamics* (North-Holland Physics, 1985).

9. M. O. Scully and M. S. Zubairy, *Quantum optics* (Cambridge University, 1997).
10. S. A. Blumenstein, "Classical ghost imaging with opto-electronic light sources: novel and highly incoherent concepts," (Technische Universität, Darmstadt, 2017).
11. D. S. Wiersma, "The physics and applications of random lasers," *Nat. Phys.* **4**(5), 359–367 (2008).
12. D. S. Wiersma, "Random lasers explained?" *Nat. Photonics* **3**(5), 246–248 (2009).
13. F. Boitier, A. Godard, E. Rosencher, and C. Fabre, "Measuring photon bunching at ultrashort timescale by two-photon absorption in semiconductors," *Nat. Phys.* **5**(4), 267–270 (2009).
14. S. Shin, U. Sharma, H. Tu, W. Jung, and S. A. Boppart, "Characterization and analysis of relative intensity noise in broadband optical sources for optical coherence tomography," *IEEE Photonics Technol. Lett.* **22**(14), 1057–1059 (2010).
15. M. Blazek, S. Hartmann, A. Molitor, and W. Elsaesser, "Unifying intensity noise and second-order coherence properties of amplified spontaneous emission sources," *Opt. Lett.* **36**(17), 3455–3457 (2011).
16. M. Blazek and W. Elsaesser, "Coherent and thermal light: Tunable hybrid states with second-order coherence without first-order coherence," *Phys. Rev. A* **84**(6), 063840 (2011).
17. S. Hartmann, A. Molitor, M. Blazek, and W. Elsaesser, "Tailored first- and second-order coherence properties of quantum dot superluminescent diodes via optical feedback," *Opt. Lett.* **38**(8), 1334–1336 (2013).
18. S. Hartmann and W. Elsaesser, "A novel semiconductor-based, fully incoherent amplified spontaneous emission light source for ghost imaging," *Sci. Rep.* **7**(1), 41866 (2017).
19. H. Carmichael, *An open systems approach to quantum optics* (Springer-Verlag, 1991).
20. M. T. Hill and M. C. Gather, "Advances in small lasers," *Nat. Photonics* **8**(12), 908–918 (2014).
21. P. E. Kloeden and E. Platen, *Numerical Solutions of Stochastic Differential Equations* (Springer-Verlag, 1992).
22. A. Pusch, S. Wuestner, J. M. Hamm, K. L. Tsakmakidis, and O. Hess, "Coherent amplification and noise in gain-enhanced nanoplasmonic metamaterials: a Maxwell-Bloch Langevin approach," *ACS Nano* **6**(3), 2420–2431 (2012).
23. P. Gartner, "Two-level laser: Analytical results and the laser transition," *Phys. Rev. A* **84**(5), 053804 (2011).
24. L. D. Landau and E. M. Lifshitz, *Statistical Physics* (Pergamon, 1980).
25. A. V. Dorofeenko, A. A. Zyablovsky, A. A. Pukhov, A. A. Lisyansky, and A. P. Vinogradov, "Light propagation in composite materials with gain layers," *Phys. Uspekhi* **55**(11), 1080–1097 (2012).
26. A. A. Zyablovsky, I. A. Nechepurenko, E. S. Andrianov, A. V. Dorofeenko, A. A. Pukhov, A. P. Vinogradov, and A. A. Lisyansky, "Optimum gain for plasmonic distributed feedback lasers," *Phys. Rev. B* **95**(20), 205417 (2017).
27. A. Kowalevich, T. Ko, I. Hartl, J. Fujimoto, M. Pollnau, and R. Salathé, "Ultrahigh resolution optical coherence tomography using a superluminescent light source," *Opt. Express* **10**(7), 349–353 (2002).
28. A. F. Fercher, W. Drexler, C. K. Hitzenberger, and T. Lasser, "Optical coherence tomography - principles and applications," *Rep. Prog. Phys.* **66**(2), 239–303 (2003).
29. T. Ko, D. Adler, J. Fujimoto, D. Mamedov, V. Prokhorov, V. Shidlovski, and S. Yakubovich, "Ultrahigh resolution optical coherence tomography imaging with a broadband superluminescent diode light source," *Opt. Express* **12**(10), 2112–2119 (2004).
30. G. A. Alphonse, D. B. Gilbert, M. G. Harvey, and M. Ettenberg, "High-power superluminescent diodes," *IEEE J. Quantum Electron.* **24**(12), 2454–2457 (1988).
31. G. A. Alphonse, "Design of high-power superluminescent diodes with low spectral modulation," in *Proc. SPIE 4648, Test and Measurement Applications of Optoelectronic Devices* (SPIE, 2002), pp. 125–139.
32. H. Weaver, D. R. W. Williams, N. H. Dieter, and W. T. Lum, "Observations of a strong unidentified microwave line and of emission from the OH molecule," *Nature* **208**(5005), 29–31 (1965).
33. V. S. Letokhov, "Laser action in stellar atmospheres," *IEEE J. Quantum Electron.* **8**(6), 615 (1972).
34. V. S. Letokhov and S. Johansson, *Astrophysical Lasers* (Oxford University, 2009).
35. M. A. Johnson, M. A. Betz, R. A. McLaren, E. C. Sutton, and C. H. Townes, "Nonthermal 10 micron CO₂ emission lines in the atmospheres of Mars and Venus," *Astrophys. J.* **208**, L145–L148 (1976).
36. M. J. Mumma, D. Buhl, G. Chin, D. Deming, F. Espenak, T. Kostiuik, and D. Zipoy, "Discovery of natural gain amplification in the 10-micrometer carbon dioxide laser bands on Mars: a natural laser," *Science* **212**(4490), 45–49 (1981).
37. N. N. Lavrinovich and V. S. Letokhov, "The possibility of the laser effect in stellar atmospheres," *Sov. Phys. JETP* **40**(5), 800–805 (1975).
38. S. Johansson and V. S. Letokhov, "Radiative cycle with stimulated emission from atoms and ions in an astrophysical plasma," *Phys. Rev. Lett.* **90**(1), 011101 (2003).
39. A. Gatti, M. Bache, D. Magatti, E. Brambilla, F. Ferri, and L. A. Lugiato, "Coherent imaging with pseudo-thermal incoherent light," *J. Mod. Opt.* **53**(5–6), 739–760 (2006).
40. F. Ferri, D. Magatti, A. Gatti, M. Bache, E. Brambilla, and L. A. Lugiato, "High-resolution ghost image and ghost diffraction experiments with thermal light," *Phys. Rev. Lett.* **94**(18), 183602 (2005).
41. A. Valencia, G. Scarcelli, M. D'Angelo, and Y. Shih, "Two-photon imaging with thermal light," *Phys. Rev. Lett.* **94**(6), 063601 (2005).
42. G. Scarcelli, A. Valencia, and Y. Shih, "Experimental study of the momentum correlation of a pseudothermal field in the photon-counting regime," *Phys. Rev. A* **70**(5), 051802 (2004).
43. X.-H. Chen, Q. Liu, K.-H. Luo, and L.-A. Wu, "Lensless ghost imaging with true thermal light," *Opt. Lett.* **34**(5), 695–697 (2009).

44. D. Zhang, Y. H. Zhai, L. A. Wu, and X. H. Chen, "Correlated two-photon imaging with true thermal light," *Opt. Lett.* **30**(18), 2354–2356 (2005).